

₁ Study of neutrino-nucleus interaction at around 1 GeV using
₂ a 3D grid-structure neutrino detector, WAGASCI, muon
₃ range detectors and magnetized spectrometer, Baby MIND,
₄ at J-PARC neutrino monitor hall

₅ A. Bonnemaison, R. Cornat, L. Domine, O. Drapier, O. Ferreira, F. Gastaldi,
₆ M. Gonin, J. Imber, M. Licciardi, F. Magniette, T. Mueller, L. Vignoli, and O. Volcy
₇ *Ecole Polytechnique, IN2P3-CNRS, Laboratoire Leprince-Ringuet, Palaiseau,*
₈ *France*

₉ S. Cao and T. Kobayashi

₁₀ *High Energy Accelerator Research Organization (KEK), Tsukuba, Ibaraki, Japan*

₁₁ M. Khabibullin, A. Khotjantsev, A. Kostin, Y. Kudenko, A. Mefodiev, O. Mineev,
₁₂ S. Suvorov, and N. Yershov

₁₃ *Institute for Nuclear Research of the Russian Academy of Sciences, Moscow, Russia*

₁₄ B. Quilain

₁₅ *Kavli Institute for the Physics and Mathematics of the Universe (WPI), The*
₁₆ *University of Tokyo Institutes for Advanced Study, University of Tokyo, Kashiwa,*
₁₇ *Chiba, Japan*

₁₈ T. Hayashino, A. Hiramoto, A.K. Ichikawa, K. Nakamura, T. Nakaya, K Yasutome,
₁₉ and K. Yoshida

₂₀ *Kyoto University, Department of Physics, Kyoto, Japan*

₂₁ Y. Azuma, J. Harada, T. Inoue, K. Kin, N. Kukita, S. Tanaka, Y. Seiya,
₂₂ K. Wakamatsu, and K. Yamamoto

₂₃ *Osaka City University, Department of Physics, Osaka, Japan*

24 A. Blondel, F. Cadoux, Y. Favere, E. Noah, L. Nicola, and S. Parsa

25 *University of Geneva, Section de Physique, DPNC, Geneva, Switzerland*

26 N. Chikuma, F. Hosomi, T. Koga, R. Tamura, and M. Yokoyama

27 *University of Tokyo, Department of Physics, Tokyo, Japan*

28 Y. Hayato

29 *University of Tokyo, Institute for Cosmic Ray Research, Kamioka Observatory,
30 Kamioka, Japan*

31 Y. Asada, K. Matsushita, A. Minamino, K. Okamoto, and D. Yamaguchi

32 *Yokohama National University, Faculty of Engineering, Yokohama, Japan*

33 December 13, 2017

34 **Contents**

35	1	Introduction	3
36	2	Experimental Setup	4
37	2.1	Wagasci module	5
38	2.2	INGRID Proton module	6
39	2.3	Baby MIND	8
40	2.3.1	Magnet modules	8
41	2.3.2	Scintillator modules	10
42	2.3.3	Electronics	11
43	2.3.4	Pefromance check	14
44	2.4	Side muon range detector	14
45	3	Physics goals	15
46	3.1	Expected number of events	17
47	3.2	Pseudo-monochromatic beam by using different off-axis fluxes	18
48	3.3	Subjects Wagasci can contribute	18

49	4 Status of J-PARC T59 experiment	20
50	5 MC studies	21
51	5.1 Detector simulation	21
52	5.1.1 Detector geometry	24
53	5.1.2 Response of detector components	24
54	5.2 Track reconstruction	25
55	5.3 Event selection	25
56	5.4 Cross section measurements on water	27
57	5.4.1 Charged current cross section measurement	27
58	6 Standalone WAGASCI-module performances	27
59	6.1 Reconstruction algorithm	29
60	6.1.1 Description	29
61	6.1.2 Performances	31
62	6.2 Background subtraction: the water-out module	38
63	7 Schedule	41
64	8 Requests	41
65	8.1 Neutrino beam	41
66	8.2 Equipment request including power line	41
67	8.2.1 Baby MIND Equipment request including power line	42
68	9 Conclusion	42

69 **1 Introduction**

70 The understanding of neutrino-nucleus interactions in the 1 GeV energy region is critical
 71 for the success of accelerator-based neutrino oscillation experiments such as the T2K exper-
 72 iment. Complicated multi-body effects of nuclei render this understanding difficult. The
 73 T2K near detectors have been measuring these and significant progress has been achieved.
 74 However, the understanding is still limited. One of the big factors preventing from full
 75 understanding is the non-monochromatic neutrino beam spectrum. Measurements with
 76 different but some overlapping beam spectra would greatly benefit to resolve the contri-
 77 bution from different neutrino energies. We, the Wagasci collaboration, proposes to study
 78 the neutrino-nucleus interaction at the B2 floor of the neutrino monitor building, where
 79 different neutrino spectra can be obtained due to the different off-axis position. Our exper-
 80 imental setup contains 3D grid-structure plastic-scintillator detectors filled with water as
 81 the neutrino interaction target (Wagasci modules), two side- and one downstream- muon
 82 range detectors(MRD's). The 3D grid-structure and side-MRD's allows a measurement of

wider-angle scattering than the T2K off-axis near detector (ND280). High water to scintillator material ratio enables the measurement of the neutrino interaction on water, which is highly desired for the T2K experiment because it's far detector, Super-Kamiokande, is composed of water. The MRD's consist of plastic scintillators and iron plates. The downstream-MRD, so called the Baby MIND detector, also works as a magnet and provides the charge identification capability as well as magnetic momentum measurement for high energy muons. The charge identification is essentially important to select antineutrino events in the antineutrino beam because contamination of the neutrino events is as high as 30%. Most of the detectors has been already constructed. The Wagasci modules have been commissioned as the J-PARC T59 experiment and the Baby MIND detector was commissioned at the CERN neutrino platform. Therefore, the collaboration will be ready to proceed to the physics data taking for the T2K beam time in January 2019. We will provide the cross sections of the charged current neutrino and antineutrino interactions on water with slightly higher neutrino energy than T2K ND280 with wide angler acceptance. When combined with ND280 measurements, our measurement would greatly improve the understanding of the neutrino interaction at around 1 GeV and contribute to reduce one of the most significant uncertainty of the T2K experiment.

2 Experimental Setup

Figure. 1 and 2 show a schematic view and a CAD drawing of the entire set of detectors. Central neutrino target detectors consist of two Wagasci modules and T2K INGRID proton module. Inside the Wagasci module, plastic scintillator bars are aligned as a 3D grid-like structure and spaces in the structure are filled with water for a water-in Wagasci module. T2K INGRID proton module is a full active neutrino target detector which is composed only with scintillator bars in its tracking region. The central detectors are surrounded by two side- and one downstream- muon range detectors(MRD's) The MRD's are used to select muon tracks from the charged-current (CC) interactions and to reject short tracks caused by neutral particles that originate mainly from neutrino interactions in material surrounding the central detector, like the walls of the detector hall, neutrons and gammas, or neutral-current (NC) interactions. The muon momentum can be reconstructed from its range inside the detector. The MRD's consist of plastic scintillators and iron plates. In addition, each of the iron plates of the downstream-MRD, so called the Baby MIND detector, is wound by a coil and can be magnetized. It provide the charge selection capability.

For all detectors, scintillation light in the scintillator bar is collected and transported to a photodetector with a wavelength shifting fiber (WLS fiber). The light is read out by a photodetector, Multi-Pixel Photon Counter (MPPC), attached to one end of the WLS fiber. The signal from the MPPC is read out by the dedicated electronics developed for the test experiment to enable bunch separation in the beam spill. The readout electronics is triggered using the beam-timing signal from MR to synchronize to the beam. The beam-

121 timing signal is branched from those for T2K, and will not cause any effect on the T2K
122 data taking.

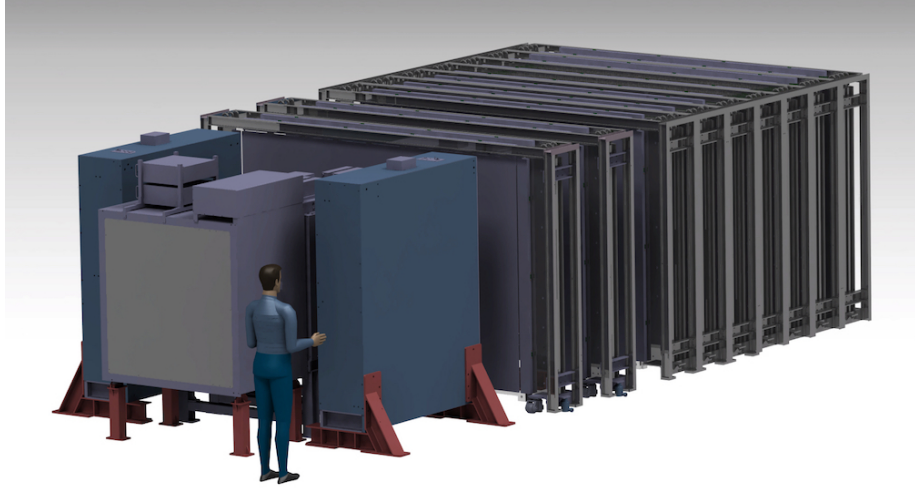


Figure 1: Schematic view of entire sets of detectors.

123 T2K adopted the off-axis beam method, in which the neutrino beam is intentionally
124 directed 2.5 degrees away from SK producing a narrow band ν_μ beam. The off-axis near
125 detector, ND280, is installed towards the SK direction in the B1 floor of the near detector
126 hall of the J-PARC neutrino beam-line. We propose to install our detector in the B2 floor
127 of the near detector hall, where the off-axis angle is similar but slightly different: 1.5 degree.
128 The candidate detector position in the B2 floor is shown in Fig. 3. The expected neutrino
129 energy spectrum at the candidate position is shown in Fig. 4.

130 **2.1 Wagasci module**

131 The Wagasci module is a neutrino target detector consists of a stainless tank filled with
132 16 scintillator tracking planes immersed, where each plane is an array of 80 scintillator
133 bars. The 40 bars, called parallel scintillators, are placed perpendicularly to the beam,
134 and the other 40 bars, called grid scintillators, are placed in parallel to the beam with grid
135 structure.

136 The dimension of the each Wagasci module is 100cm \times 100cm in the x and y directions
137 and 50cm along the beam direction. Thin plastic scintillator bars (thickness \sim 0.3cm)
138 are used for the Wagasci module to reduce the mass ratio of scintillator bars to water,
139 because neutrino interactions in the scintillator bars are a background for the cross section
140 measurements.

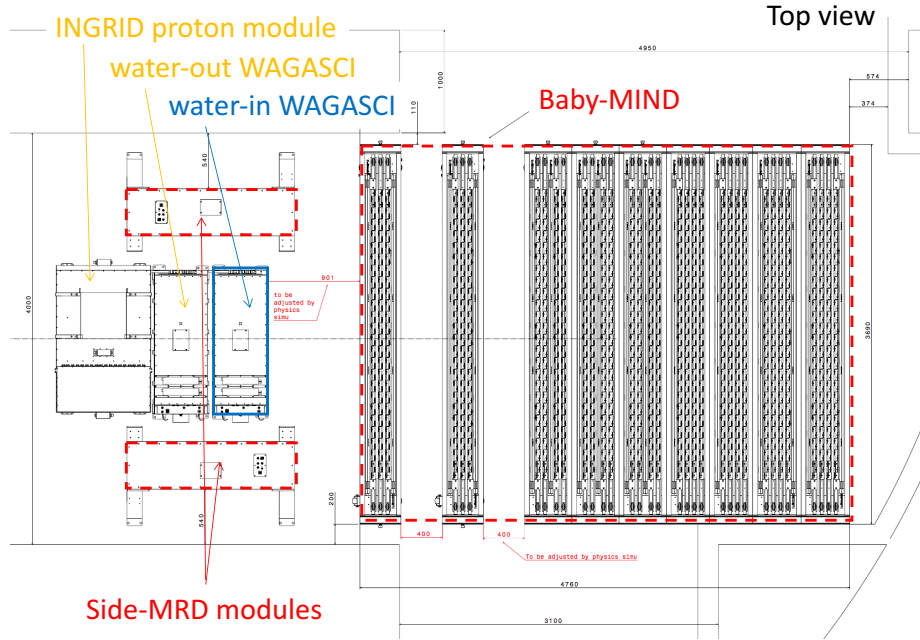


Figure 2: Top view of entire sets of detectors.

141 Inside the Wagasci module, plastic scintillator bars are aligned as a 3D grid-like struc-
142 ture, shown in Fig. 9.

143 Spaces in the 3D grid-like structure are filled with water for the water-in Wagasci
144 module. The total water mass serving as neutrino targets in the detector are ~ 0.5 ton.

145 When neutrinos interact with hydrogen, oxygen or carbon, in water and scintillators,
146 charged particles are generated. Neutrino interactions are identified by detecting tracks of
147 charged particles through plastic scintillation bars. Thanks to the 3 D grid-like structure
148 of the scintillator bars, the Wagasci module has 4π angular acceptance for charged parti-
149 cles. Furthermore, adopting a 5cm grid spacing, short tracks originated from protons and
150 charged pions can be reconstructed with high efficiency.

151 Scintillator bars whose dimensions are 2.5cm x 0.3cm x 100cm are used for the Wagasci
152 module. The total number of channels in one Wagasci module is 1280.

153 2.2 INGRID Proton module

154 INGRID Proton module is a neutrino detectors of the T2K experiment. It is composed only
155 with scintillator bars in its tracking region. (Add more explanation here.) It was installed
156 at the neutrino beam axis on the SS floor of the T2K near detector hall in 2010, and had

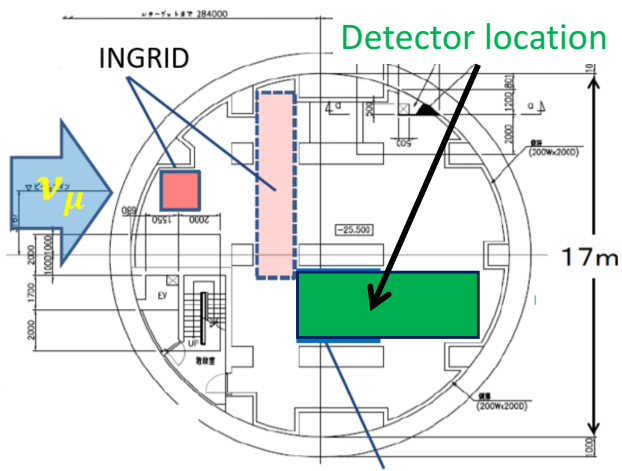


Figure 3: Candidate detector position in the B2 floor of the near detector hall.

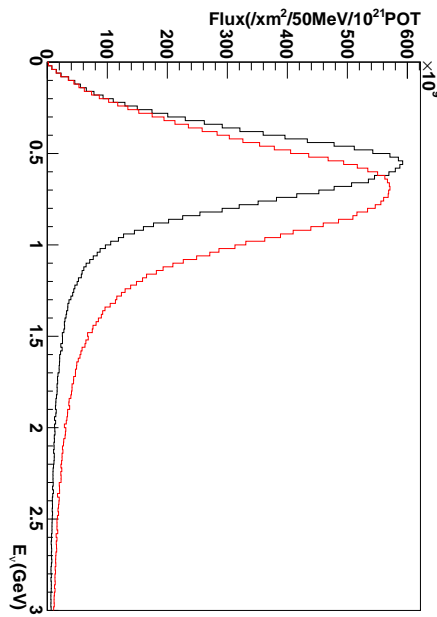


Figure 4: Neutrino energy spectrum at the candidate detector position(red, off-axis 1.5 degree). The spectrum at the ND280 site (black, off-axis 2.5 degree) is also shown.

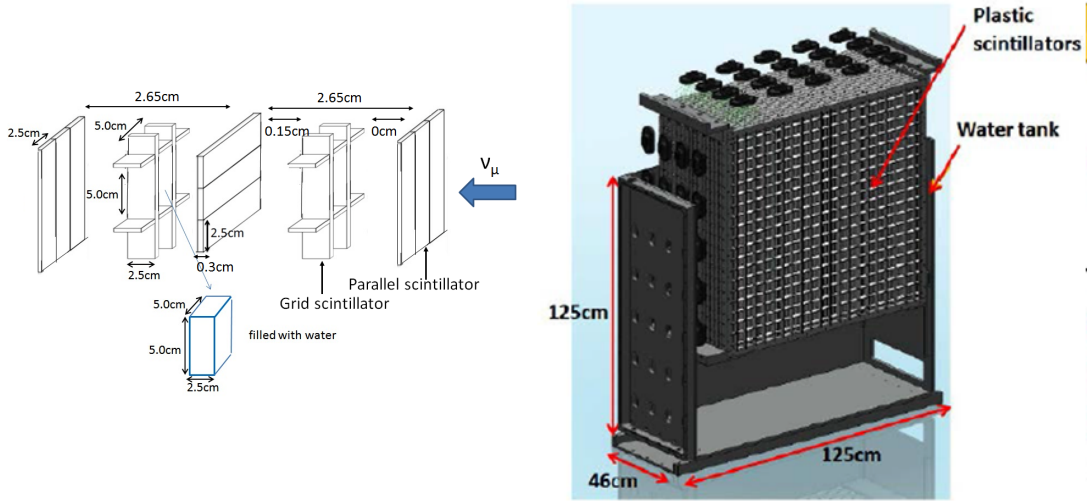


Figure 5: 2D track reconstruction efficiency as a function of number of hits (left) and track angle (right). Here the track angle is the one reconstructed by the INGRID module.

157 been used for neutrino cross section measurements. In August 2017, it was moved to the
 158 B2 floor of the same detector hall by J-PARC T59 after getting the approval from T2K
 159 to use them. J-PARC T59 is performing neutrino beam measurement using the detector
 160 from October 2017, and the measurement will continue until May 2018.

161 **2.3 Baby MIND**

162 The Baby MIND is the downstream Muon Range Detector. It also works as a magnet and
 163 provides the charge identification capability as well as magnetic momentum measurement
 164 for high energy muons.

165 The Baby MIND collaboration ¹ submitted a proposal to the SPSC at CERN, SPSC-P-
 166 353. The project was approved by the CERN research board as Neutrino Platform project
 167 NP05 and constructed. The detector consists of 33 magnet modules, each 3500 mm ×
 168 2000 mm × 50 mm (30 mm steel) with a mass of approximately 2 tonnes. Of these magnet
 169 modules, 18 are instrumented with plastic scintillator modules.

170 **2.3.1 Magnet modules**

171 The Baby MIND is built from sheets of iron interleaved with scintillator detector modules
 172 but unlike traditional layouts for magnetized iron neutrino detectors (e.g. MINOS) which

¹Contact person: E. Noah, Spokesperson: A. Blondel, Deputy spokesperson: Y. Kudenko

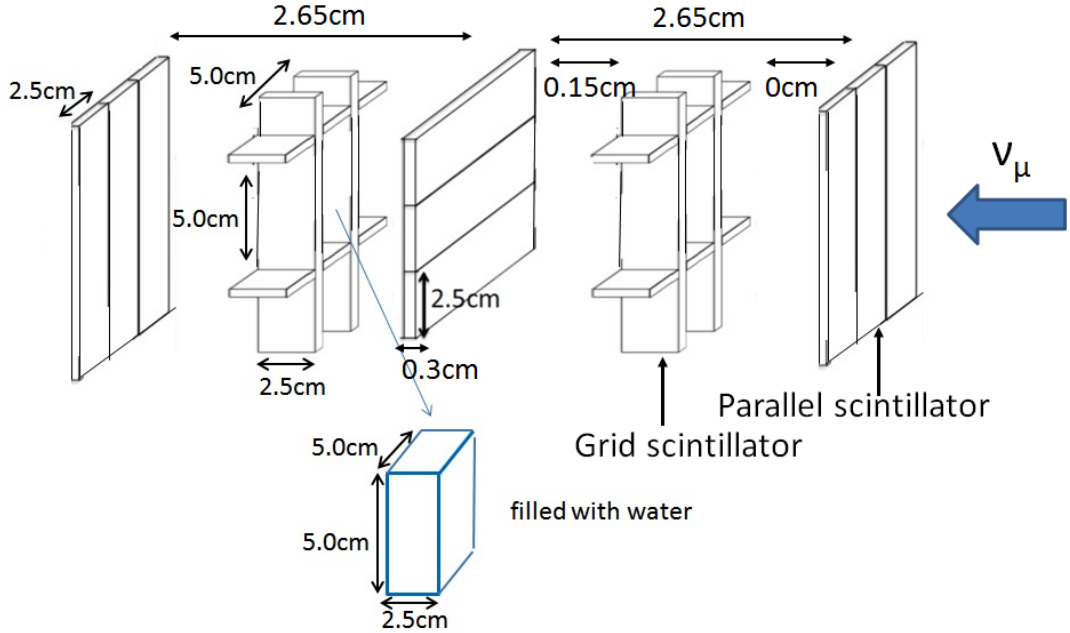


Figure 6: Schematic view of 3D grid-like structure of plastic scintillator bars inside the central detector.

tend to be monolithic blocks with a unique pitch between consecutive steel segments and large conductor coils threaded around the whole magnet volume, the Baby MIND iron segments are all individually magnetized as shown in Fig. 10, allowing for far greater flexibility in the setting of the pitch between segments, and in the allowable geometries that these detectors can take.

The key design outcome is a highly optimized magnetic field map. A double-slit configuration for coil winding was adopted to increase the area over which the magnetic flux lines are homogeneous in B_x across the central tracking region. Simulations show the magnet field map to be very uniform over this central tracking region covering an area of $2800 \times 2000 \text{ mm}^2$, Fig. 11. The B_x component dominates in this region, with negligible B_y and B_z . This was confirmed by measuring the field with 9 pick-up coils wound around the first module. Subsequent modules were equipped with one pick-up coil. Test results on the 33 modules show all to achieve the required field of 1.5 T for a current of 140 A, with a total power consumption of 11.5 kW. The polarity of the field map shown in Fig. 11 (middle) can be reversed by changing the power supply configuration.

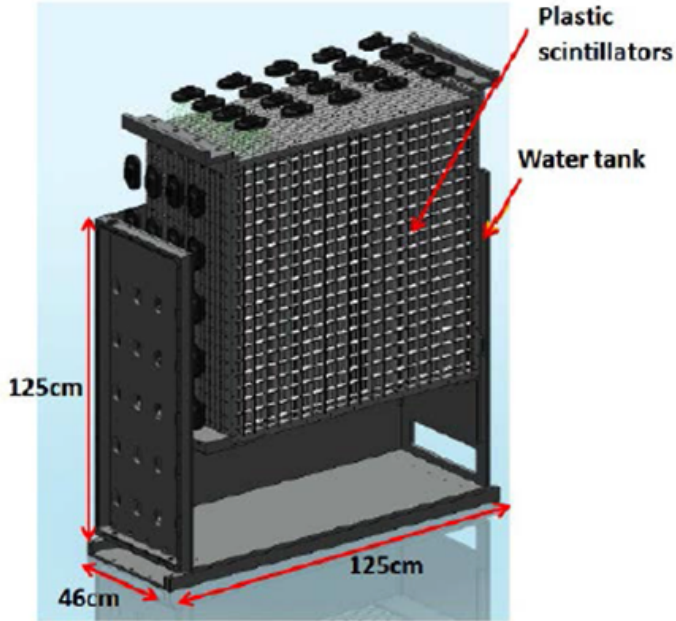


Figure 7: Schematic view of Wagasci module.

188 2.3.2 Scintillator modules

189 Each of the 18 scintillator modules is constructed from 2 planes of horizontal counters (95
 190 counters in total) and 2 planes of vertical counters (16 counters in total) [2], arranged
 191 with an overlap between planes to achieve close to 100% hit efficiency for minimum ionizing
 192 muons. The arrangement of planes within a module is vertical-horizontal-horizontal-
 193 vertical. This arrangement was the result of an assembly approach whereby each plane
 194 was built from 2 half-planes, with each half plane consisting of a horizontal plane and a
 195 vertical plane. The scintillator bars are held in place using structural ladders that align
 196 and maintain the counters, Fig. 12. No glue is used in the process, so counters can be
 197 replaced. Aluminum sheets front and back provide light tightness.

198 The plastic scintillator counters were made from 220 mm-wide slabs, consisting of
 199 extruded polystyrene doped with 1.5% paraterphenyl (PTP) and 0.01% POPOP. They were
 200 cut to size then covered with a 30-100 μm thick diffuse reflector resulting from etching of
 201 the surface with a chemical agent [4, 5]. The horizontal counter size is $2880 \times 31 \times 7.5 \text{ mm}^3$,
 202 with one groove along the length of the bar in which sits a wavelength shifting fiber from
 203 Kuraray. The vertical counter size is $1950 \times 210 \times 7.5 \text{ mm}^3$, with one U-shaped groove
 204 along the bar. On each counter, two custom connectors house silicon photomultipliers,
 205 MPPC type S12571-025C from Hamamatsu, either side of the horizontal counter, and

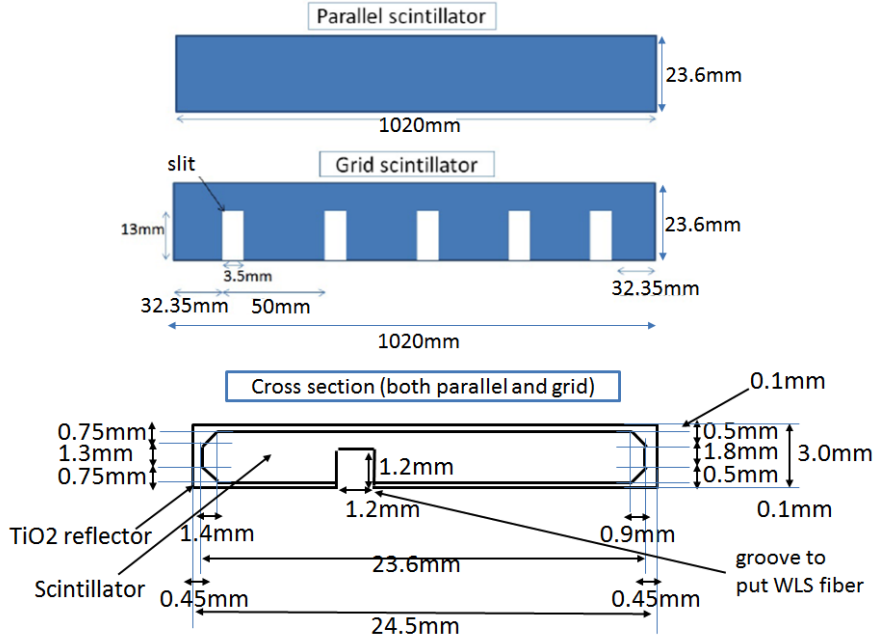


Figure 8: Geometry of scintillators used for Wagasci modules.

206 both connectors at the top for the vertical counter. This geometrical configuration for
 207 vertical counters was chosen for ease of connectivity to the electronics, and maintenance
 208 operations.

209 A total of 1744 horizontal counters and 315 vertical counters (including spares) were
 210 produced at the Uniplast company (Vladimir, Russia).

211 2.3.3 Electronics

212 The Baby MIND electronic readout scheme includes several custom-designed boards [6].
 213 The revised version is shown in Fig. 13. At the heart of the system is the electronics
 214 Front End Board (FEB), developed by the University of Geneva. The readout system
 215 includes two ancillary boards, the Backplane, and the Master Clock Board (MCB) whose
 216 development has been managed by INRNE (Bulgarian Academy of Sciences) collaborators.

217 The FEBv2 hosts 3 CITIROC chips that can each read in signals from 32 SiPMs [3].
 218 Each signal input is processed by a high gain, and a separate low gain, signal path. The
 219 outputs from the slow shapers can be sampled using one of two modes: a mode with an
 220 externally applied delay, and a peak detector mode. A faster shaper can be switched to
 221 either HG or LG paths, followed by discriminators with adjustable thresholds providing 32
 222 individual trigger outputs and one OR32 trigger output. An Altera ARIA5 FPGA on the

tmp.pdf

Figure 9: tmp.

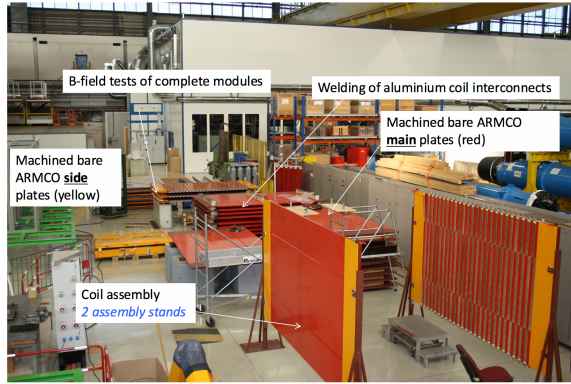


Figure 10: Magnet assembly zone at CERN.

223 FEBv2 samples these trigger outputs at 400 MHz, recording rising and falling times for
224 the individual triggers and assigning time stamps to these. Time-over-threshold from the
225 difference between falling and rising times gives some measure of signal amplitude, used in
226 addition to charge information and useful if there is more than one hit per bar within the
227 deadtime due to the readout of the multiplexed charge output of $\sim 9 \mu\text{s}$. The ARIA5 also
228 manages the digitization of the sampled CITIROC multiplexed HG and LG outputs via a
229 12-bit 8-ch ADC.

230 The internal 400 MHz clock on the FEBv2 can be synchronized to a common 100 MHz
231 clock. The synchronization subsystem combines input signals from the beam line into
232 a digital synchronization signal (SYNC) and produces a common detector clock (CLK)
233 which can eventually be synchronised to an external experiment clock. Both SYNC and
234 CLK signals are distributed to the FEBs. Tests show the FEB-to-FEB CLK(SYNC) delay
235 difference to be 50 ps (70 ps). Signals from the beam line at WAGASCI include two

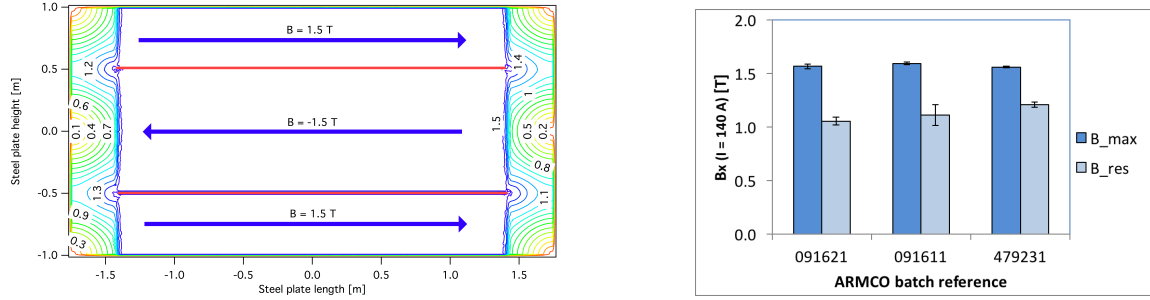


Figure 11: Left) Magnetic field map with a coil along 280 cm of the length of the plate. Right) Measured B field for 33 modules.



Figure 12: Scintillator modules assembly. Left) top of front half-module showing vertical counters, and the spacers-ladders that set the pitch between horizontal counters and hold them in place. Middle) rear half-module showing horizontal counters on their ladders. Right) Assembled rear half-module, the front half-module can be seen in the background.

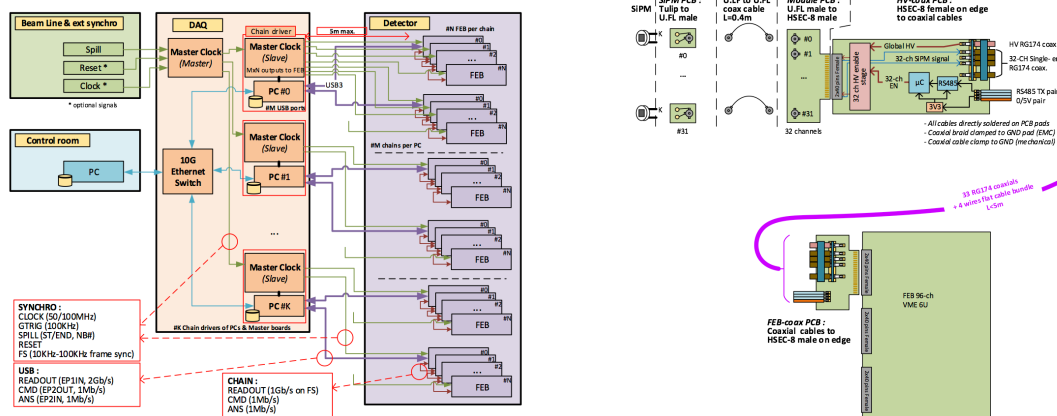


Figure 13: Left) Baby MIND electronics readout scheme. Right) SiPM-to-FEB connectivity.

236 separate timing signals, arriving 100 ms and 30 μ s before the neutrino beam at the near
 237 detectors. The spill number is available as a 16-bit signal.

238 2.3.4 Pefromance check

239 All counters were measured at INR Moscow with a cosmic ray setup using the same type
 240 S12571-025C MPPCs and CAEN DT5742 digitizer. The average light yield (sum from both
 241 ends) was measured to be 37.5 photo-electrons (p.e.) per minimum ionizing particle (MIP)
 242 and 65 p.e./MIP for vertical and horizontal counters, respectively. After shipment to
 243 CERN, all counters were tested once more individually with an LED test setup [?]. 0.1% of
 244 counters failed the LED tests and were therefore not used during the assembly of modules.
 245 The assembly of modules was completed in June 2017, and it was then tested in June and
 246 July 2017 at the Proton Synchrotron experimental hall at CERN with a mixed particle
 247 beam comprising mostly muons whose momenta could be selected between 0.5 and 5 GeV/c.
 An event display from the summer 2017 tests is shown in Fig. 14.

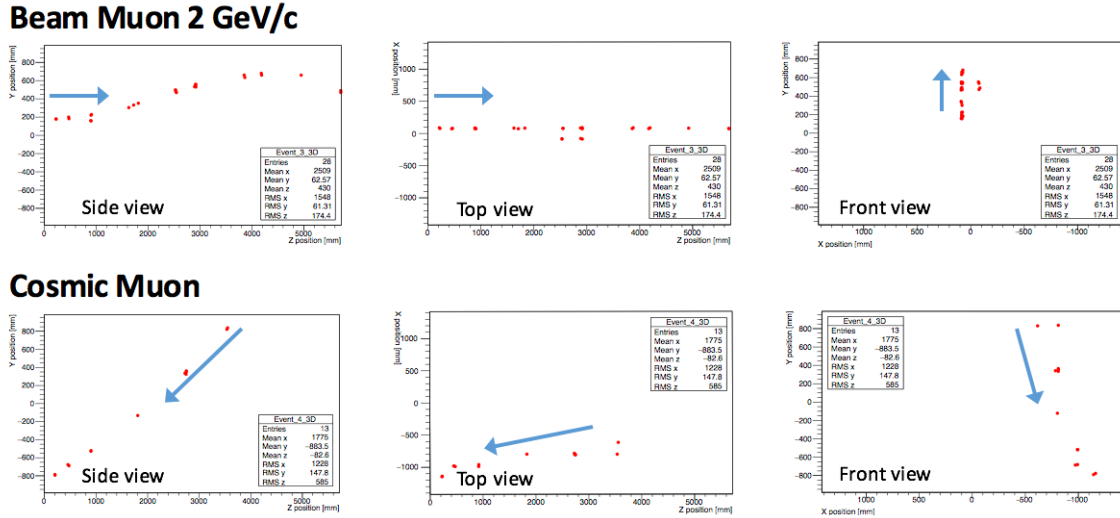


Figure 14: Comparison of a beam muon and cosmic muon in the three different geometrical projections of the detector. The beam impinges on the detector from the left. The arrows indicate the direction of travel of these muons. The direction of the cosmic muon is inferred from timing information.

248

249 2.4 Side muon range detector

250 Two Side-MRD modules for tracking secondary particles from neutrino interactions will be
 251 installed in 2018. Each Side-MRD module is composed of 11 steel plates and 10 layers of

252 total 80 scintillator slabs installed in 13 mm gaps between the 30 mm thick plates. Each
253 steel plate size is $30 \times 1610 \times 1800$ mm³. Total module size is $2236 \times 1630 \times 975$ mm³ as
254 shown in Fig. 15 (left), weight is ~ 8.5 ton.

255 Scintillator bars were manufactured by Uniplast company in Vladimir, Russia. Polystyrene
256 based scintillators were extruded with thickness of 7 mm, then cut to the size of $7 \times 200 \times$
257 1800 mm³. Dopant composition is 1.5% PTP and 0.01% POPOP. Scintillator surface was
258 etched by a chemical agent to form a white diffuse layer with excellent reflective perfor-
259 mance. Ideal contact between the scintillator and the reflector raises the light yield up to
260 50% comparing to an uncovered scintillator. Sine like groove was milled along the scin-
261 tillator to provide uniform light collection over the whole scintillator surface. WLS Y11
262 Kuraray fiber of 1 mm diameter is glued with an optical cement EJ-500 in the S-shape
263 groove as shown in Fig. 15(right). Bending radius is fixed to 30 mm that was specified to
264 be safe for Kuraray S-type fibers. Both ends of the fiber are glued into optical connectors
265 which mounted within a scintillator body and provide an interface to SiPMs, Hamamatsu
266 MPPC S13081-050CS(X1).

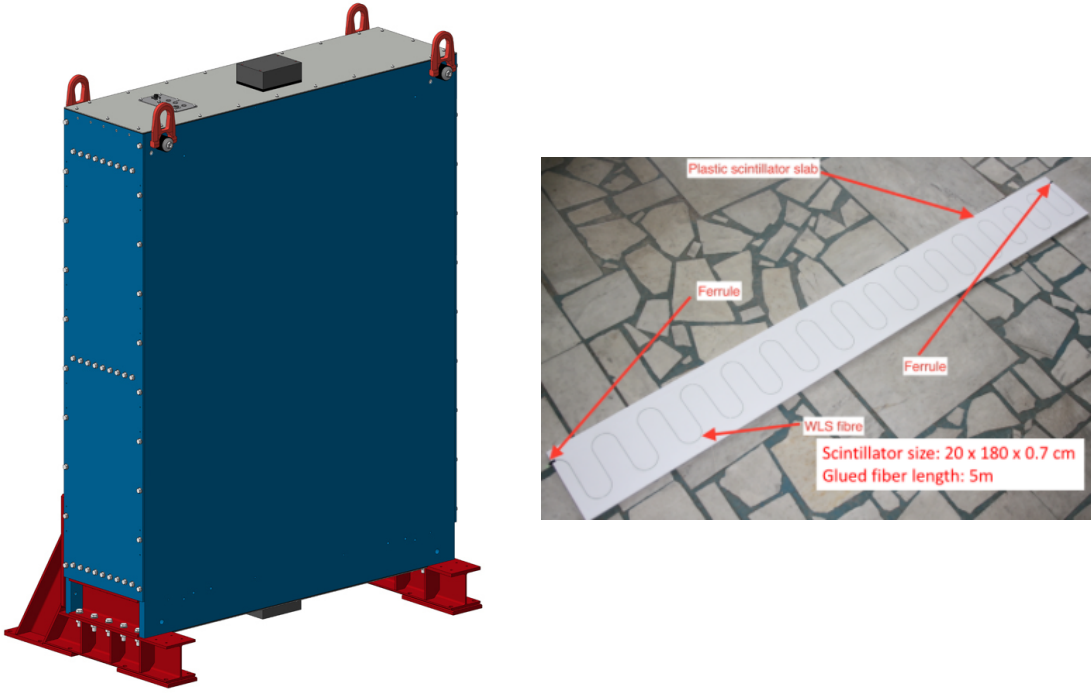


Figure 15: Left :Side-MRD module. Right: Scintillator bar of the Side-MRD modules.

267 Scintillators for the Side-MRD modules had been assembled at INR in Russia, and

268 shipped to Japan in July 2017. The light yield for each scintillator was measured with
 269 cosmic rays at INR and at YNU in Japan after delivery. Parameters measured at the
 270 center of the counter were : the light yields LY_1 and LY_2 at both ends, the light yield
 271 asymmetry between the ends calculated as $100\% \times \frac{LY_1 - LY_2}{LY_1 + LY_2}$. After tests at INR we selected
 272 324 counters from measured 332 ones with the mean light yield of 45 p.e./MIP ($LY_1 + LY_2$)
 273) and the asymmetry value less than 10 %. The measuremens at YNU yielded the average
 274 total light yield of about 40 p.e./MIP which varies in range from 32 to 50 p.e./MIP (Fig.
 275 16 (left)). Only two counters showed relatively high asymmetry close to 25 % as shown in
 276 Fig. 16 (right). Using the results of the quality assurance test we selected 320 scintillator
 277 counters for the Side-MRD modules.

278 We also measured the time resolution for a combination of four counters piled each on
 279 another one. The average result for four counters is $\sigma_T = 1.04$ ns. The resolution of com-
 280 bination of 2, 3, 4 counters is measured to be 0.79 ns, 0.66 ns and 0.58 ns, correspondently.

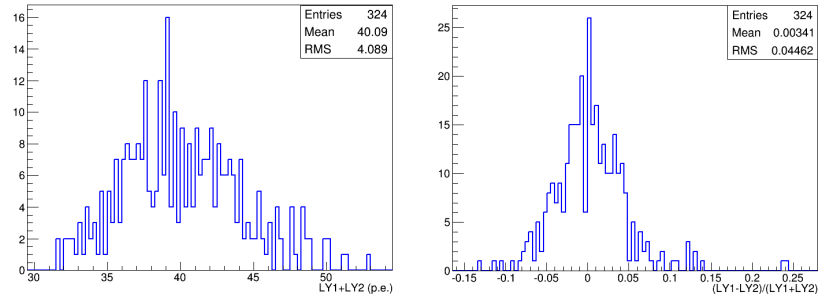


Figure 16: Total light yield distribution (left) and light yield assymetry (right) measured at YNU.

281
 282 Construction of Side-MRD modules will be done from November 2017 at Yokohama
 283 National University, then they will be transported to J-PARC and will be installed at B2
 284 floor of the T2K near detector hall.

285 3 Physics goals

286 We will measure the differential cross section for the charged current interaction on H_2O
 287 and Hydrocarbon(CH)). The water-scintillator mass ratio of the Wagasci module is as
 288 high as 5:1 and the high purity measurement of the cross section on H_2O is possible. One
 289 experimental option is to remove water from one of the two Wagasci modules. The water-
 290 out WAGASCI module will allow to measure pure-CH target interactions with very low
 291 momentum-threshold for protons. It will also benefit to subtract the background from

interaction with scintillator in the water target measurement. Another option is to add the T2K proton module which is fully made of plastic scintillators. It will allow the high statistics comparison of cross section between H₂O and CH and also comparison with the ND280 measurement. The actual configuration will be optimized with detailed MC simulation by 2018 Summer.

Our setup allows the measurements of inclusive and also exclusive channels such as 1- μ , 1- $\mu 1p$, 1- $\mu 1\pi \pm np$ samples, former two of which are mainly caused by the quasi-elastic and 2p2h interaction and the latter is mainly caused by resonant or coherent pion production and deep elastic scattering. In general, an accelerator produced neutrino beam spectrum is wide and the energy reconstruction somehow rely on the neutrino interaction model. Therefore, recent neutrino cross section measurement results including those from T2K are given as a flux-integrated cross section rather than cross sections as a function of the neutrino energy to avoid the model dependency. We can provide the flux-averaged cross section. In addition, by combining our measurements with those at ND280, model-independent extraction of the cross section for narrow energy region becomes possible. This method was demonstrated in [1] and also proposed by P** (NUPRISM).

3.1 Expected number of events

Expected number of neutrino events after the event selections is evaluated with Monte Carlo simulations as we will discuss in Section 5. In the neutrino-mode, 4.2×10^3 , 1.1×10^3 and $\sim 3.8 \times 10^3$ CC neutrino events are expected in the water-in WAGASCI module, the water-out WAGASCI module and the INGRID proton module after the selections with 0.5×10^{21} POT, and its purities are 78.0 %, 97.5 % and $\sim 98\%$. In the antineutrino-mode, 1.7×10^3 , 0.4×10^3 and $\sim 1.5 \times 10^3$ CC antineutrino events are expected in the water-in WAGASCI module, the water-out WAGASCI module and the INGRID proton module after the selections with 0.5×10^{21} POT, and its purities are 59.5 %, 74.4 % and $\sim 74\%$.

Statistical errors of flux integrated CC-inclusive neutrino cross section measurements on H₂O (full acceptance) and CH targets (forward acceptance) will be $\sim 1.5\%$ and $\sim 1.6\%$ with 0.5×10^{21} POT in the neutrino-mode. Statistical errors of flux integrated CC-inclusive antineutrino cross section measurements on H₂O (full acceptance) and CH targets (forward acceptance) will be $\sim 2.4\%$ and $\sim 2.5\%$ with 0.5×10^{21} POT in the antineutrino-mode.

Statistical errors of flux integrated H₂O to CH CC-inclusive neutrino cross section ratio measurement will be $\sim 3.1\%$ (full acceptance) and $\sim 2.3\%$ (forward acceptance) with 0.5×10^{21} POT in the neutrino-mode. Statistical errors of flux integrated H₂O to CH CC-inclusive antineutrino cross section ratio measurement will be $\sim 5\%$ (full acceptance) and $\sim 3.7\%$ (forward acceptance) with 0.5×10^{21} POT in the antineutrino-mode.

327 **3.2 Pseudo-monochromatic beam by using different off-axis fluxes**

328 The off-axis method gives narrower neutrino spectrum, and the peak energy is lower for
 329 larger off-axis angle. There still remains high energy tail mainly due to neutrinos from
 330 Kaon decay. The off-axis angle of the Wagasci location is 1.5 degree and different from the
 331 ND280 2.5 degree. Top two plots of Fig. 17 show the energy spectra of fluxes and neutrino
 332 interaction events at these two different location. The high energy tail of ND280 flux can
 333 be somehow subtraction by using the Wagasci measurement. The low energy part of the
 334 Wagasci flux can be also subtracted by using the ND280 measurement. Bottom two plots
 335 of Fig. 17 demonstrate this method. We can effectively get two fluxes, from 0.2 GeV to
 336 0.9 GeV and 0.6 GeV and 2 GeV and measure flux-integrated cross section for these two
 337 fluxes.

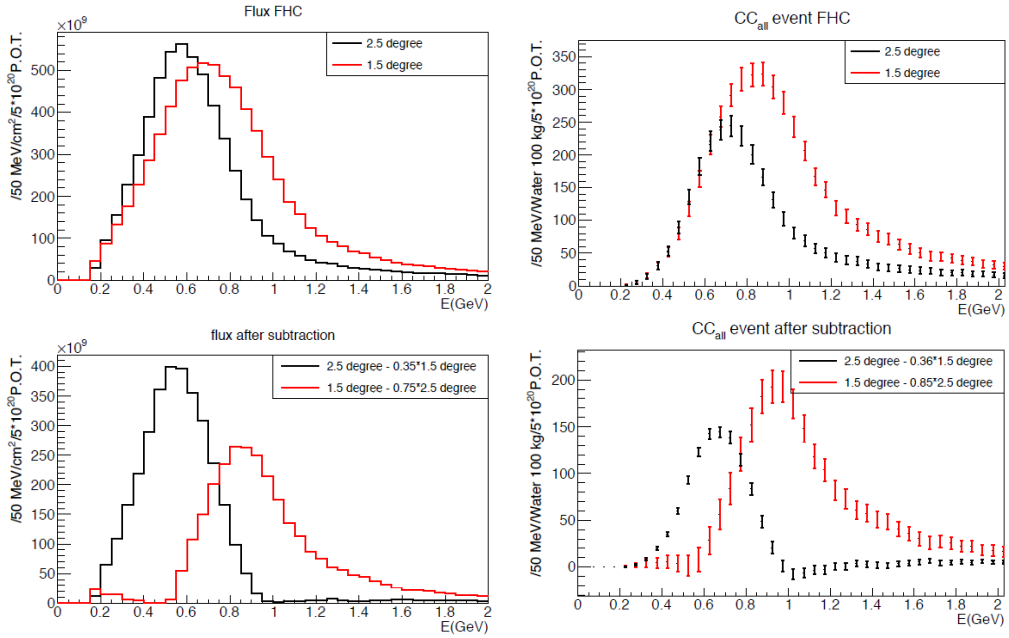


Figure 17: Energy spectra obtained by using different off-axis angle fluxes. Top two plots show the fluxes(left) and spectra of interaction events (right) for ND280 (off-axis 2.5 degree) and Wagasci (off-axis 1.5 degree). Bottom two plots show the fluxes (left) and spectra of interaction events (right) obtained by subtraction of fluxes at ND280 and Wagasci. The error bar is for the statistical error and those in the bottom right plot is obtained assuming the statistical error for ND280 measurement is much smaller than that of Wagasci experiment.

338 Statical errors of flux integrated CC-inclusive neutrino cross section measurements

339 on H₂O (forward acceptance) and CH targets (forward acceptance) with the pseudo-
340 monochromatic beam will be $\sim 2\%$ and $\sim 1.9\%$ with 0.5×10^{21} POT in the neutrino-
341 mode. Statical errors of flux integrated CC-inclusive antineutrino cross section measure-
342 ments on H₂O (full acceptance) and CH targets (forward acceptance) with the pseudo-
343 monochromatic beam will be $\sim 3\%$ and $\sim 2.8\%$ with 0.5×10^{21} POT in the neutrino-
344 mode.

345 **3.3 Subjects Wagasci can contribute**

346 In T2K experiment, neutrinos interact with bound nucleons in relatively heavy nuclei
347 (Carbon and Oxygen), so the cross-section is largely affected by nuclear effects. The nuclear
348 effects are categorized as nucleons' momentum distribution in nucleus, interactions with
349 correlated pairs of nucleons in nucleus (two particles-two holes, 2p2h), collective nuclear
350 effects calculated with Random Phase Approximation (RPA) and final state interactions
351 (FSI) of secondary particles in the nuclei after the initial neutrino interactions.

352 The 2p2h interactions mainly happen through Δ resonance interactions following a
353 pion-less decay and interactions with a correlated nucleon pair. The 2p2h interactions are
354 observed in electron scattering experiments (add ref. here) where the 2p2h events observed
355 in the gap between Quasi-Elastic region and Pion-production region as shown in Fig. ??.
356 Neutrino experiments also attempt to measure the 2p2h interactions, but separation of the
357 QE peak and the 2p2h peak is more difficult because transferred momentum (p) and energy
358 (w) are largely affected by neutrino energies which cannot be determined event-by-event in
359 the wide energy spectrum of the accelerator neutrino beam. Our model-independent narrow
360 neutrino spectra extracted from combined analyses of our data and ND280 data are ideal
361 for searching the 2p2h interaction because clearer separation of the QE peak and the 2p2h
362 peak is expected. Another way to observe the 2p2h interaction is direct measurement of
363 proton tracks in CC0 π sample with low detection threshold and full acceptance. Fig. ??
364 shows proton multiplicities in CCQE events and 2p2h events, and Fig. ?? shows opening
365 angles among two proton tracks in the same samples. The water-out WAGASCI can provide
366 good sample for the 2p2h interaction search because its low density medium enables the
367 detection of low momentum protons in addition to the full acceptance.

368 The corrections from collective nuclear effects calculated by RPA as a function of Q^2 are
369 shown in Fig. ?? . The Q^2 dependence of the correction can be tested by measuring angular
370 distribution of muons in CC1- μ and CC1- $\mu 1p$ events. The uncertainties of the corrections
371 in low (high) Q^2 regions can be constrained by observing the events with a forward-going
372 (high-angle) muon, so it is essential to measure muon tracks with full acceptance.

373 T2K experiment is starting to use ν_e CC1 π events for its CP violation search to increase
374 the statistics. One of the biggest uncertainty of the CC1 π sample comes from the final
375 state interactions of pions in the nuclei after the initial neutrino interactions because they
376 change the multiplicity, charge and kinematics of the pions. The multi-pion production
377 events can be migrated into the CC1 π sample due to the FSIs, and they become important

378 backgrounds. We can constrain the uncertainties from the pion FSIs by measuring pion
 379 rescattering in the detector and pion multiplicity in ν_μ CCn π sample with low detection
 380 threshold and full acceptance for pion tracks. The water-out WAGASCI can provide good
 381 sample for the pion FSI studies because its low density medium enables the detection of
 382 low momentum pions in addition to the full acceptance.

383 4 Status of J-PARC T59 experiment

384 We had submitted a proposal of a test experiment to J-PARC in April 2014 to test a new
 385 detector with a water target, WAGASCI, at the neutrino monitor hall, and the proposal
 386 was approved as J-PARC T59. The project contains the side and downstream muon range
 387 detectors as well.

388 The first WAGASCI module has been constructed in 2016 and installed at the on-
 389 axis position in front of the T2K INGRID detector for the commissioning and the first
 390 cross section measurement as a part of the T2K experiment. The INGRID electronics
 391 boards are used to read the signal. The light yield measured with muons produced by
 392 the interaction of neutrinos in the hall wall, shown in Fig. 18, is sufficiently high to get
 good hit efficiency. A track search algorithm based on the cellular automaton has been

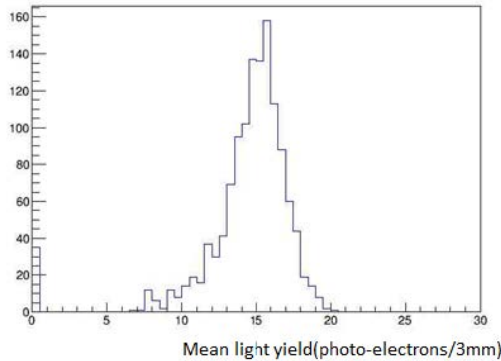


Figure 18: Light yield for muons produced by the interaction of neutrinos in the hall wall. Average light yields for each channel are plotted.

393 developed using the software tools by the T2K INGRID. Examples of observed events are
 394 shown in Fig. 19. The tracking efficiency in 2-dimensional projected plane was evaluated
 395 by comparing the reconstructed track in the WAGASCI module and the INGRID module
 396 and shown in Fig. 20. Note that the tracking efficiency for high angle (> 70 deg) is not
 397 evaluated because of the acceptance of the INGRID module, not because of the limitation
 398 of the WAGASCI module.

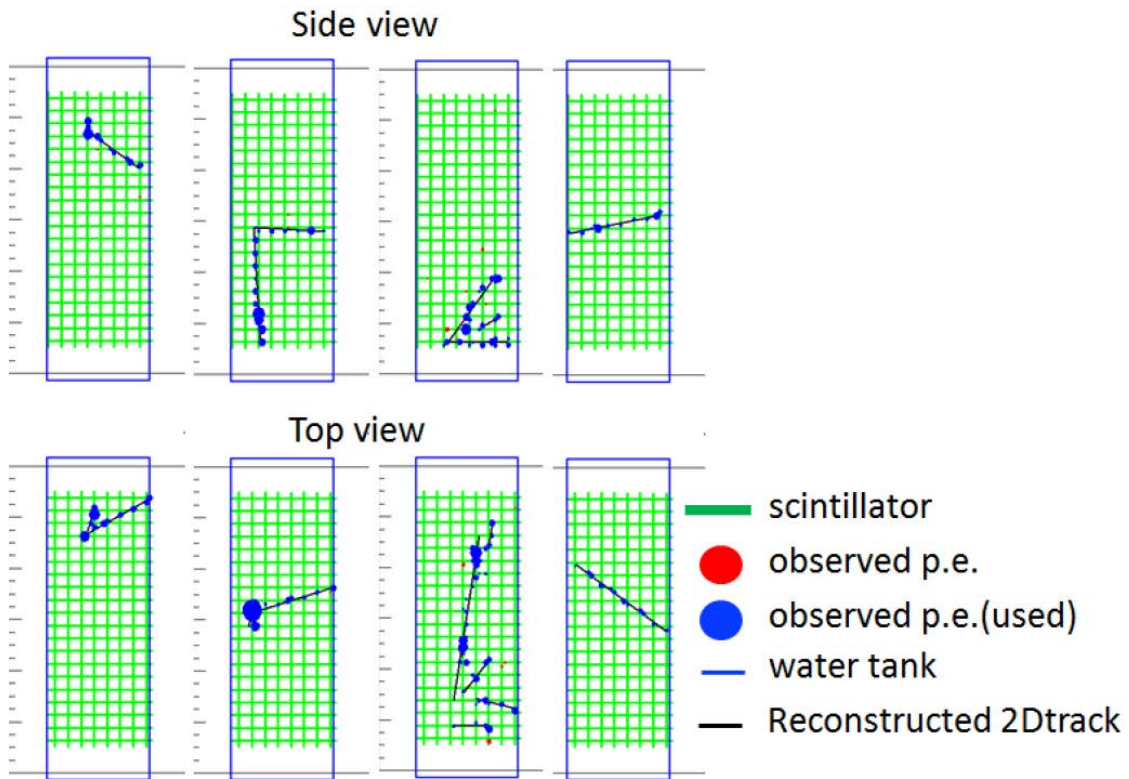


Figure 19: Example event displays of the WAGASCI module at on-axis. The reconstructed tracks are overlaid.

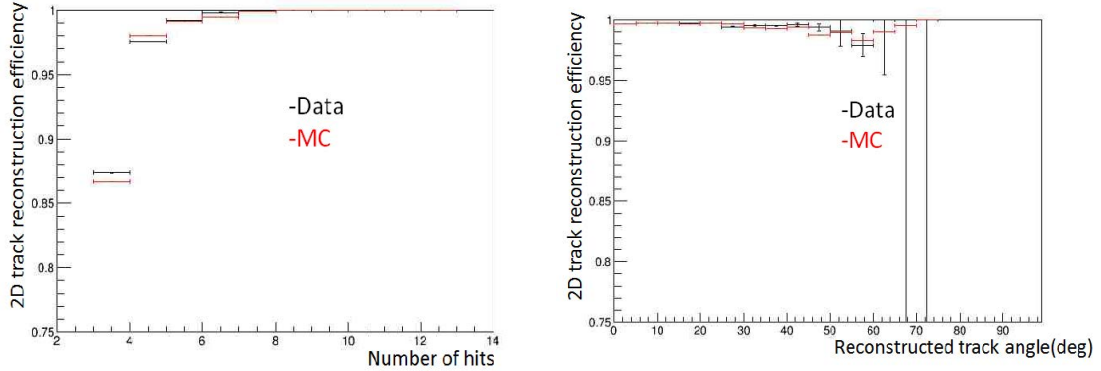


Figure 20: 2D track reconstruction efficiency as a function of number of hits (left) and track angle (right). Here the track angle is the one reconstructed by the INGRID module.

400 In 2017 Autumn, the construction of the second WAGASCI module and the dedicated
 401 electronics board were completed. The module and the electronics were install to the B2
 402 floor together with the T2K proton module and the INGRID module as shown in Fig. 21.
 403 The proton module is to be used as the entering muon veto and also for the comparison
 404 of interaction between CH and Water. The INGRID module is for the temporary muon
 405 detector with limited acceptance for this period. The detector was commissioned and is
 406 in operation to take data with the antineutrino beam during the T2K beam time from
 407 October.

408 The production of the components of the side muon range detectors has been completed
 409 and now the detectors are being assembled at the Yokohama National University. These
 410 detectors will be installed sometime from January to June, 2018 when T2K is not running.

411 The Baby MIND detector was transported from CERN to Japan in December, 2017.
 412 It will be installed and commissioned in Jan.-Feb. 2018 and T59 will take the neutrino-
 413 induced muon data in April and May.

414 5 MC studies

415 5.1 Detector simulation

416 Expected number of neutrino events in the water-in Wagasci detector is evaluated with
 417 Monte Carlo simulations. Neutrino beam flux at the detector location is simulated by
 418 T2K neutrino flux generator, JNUBEAM, neutrino interactions with target materials are
 419 simulated by a neutrino interaction simulator, NEUT, detector responses are simulated
 420 using GEANT4-based simulation. The neutrino flux at the detector location, 1.5 degrees

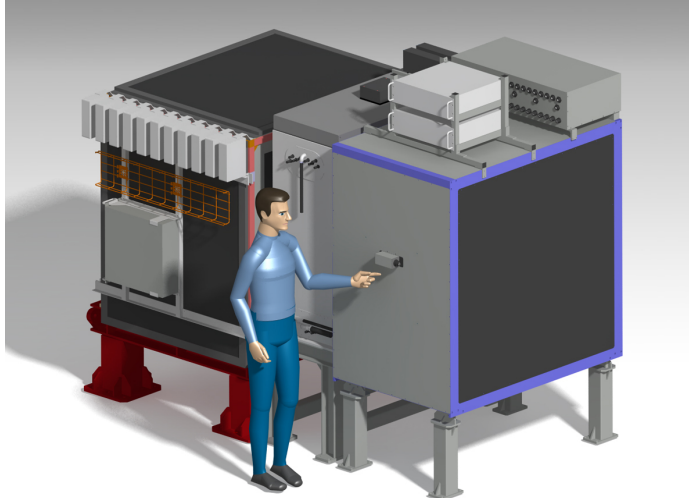


Figure 21: J-PARC T59 detector configuration in October 2017.

421 away from the J-PARC neutrino beam axis, is shown in Figure 4, and its mean neutrino
 422 energy is around 0.68 GeV.

423 **5.1.1 Detector geometry**

424 The detector geometry in the GEANT4-based simulation is slightly different from the actual
 425 detector as shown in Fig. 22. The active neutrino target region consists of four Wagasci
 426 modules, and each Wagasci detector has the dimension with 100 cm × 100 cm in the x and
 427 y directions and 50 cm along the beam direction. Two Side-MRD modules is installed at
 428 both sides of the Wagasci modules, and each Side-MRD module consists of ten iron plates
 429 whose dimension is 3 cm (thickness) × 200 cm (height) × 320 cm (width). The distance
 430 between the Side-MRD modules and Wagasci modules is 80 cm. The downstream-MRD
 431 equivalent to the Baby-MIND is installed at the downstream of the Wagasci modules. The
 432 downstream-MRD consists of thirty iron plates whose dimension is 3 cm (thickness) × 200
 433 cm (height) × 400 cm (width). The distance between the downstream-MRD modules and
 434 Wagasci modules is 80 cm.

435 **5.1.2 Response of detector components**

436 The energy deposit inside the scintillator is converted into the number of photons. The
 437 effects of collection and attenuation of the light in the scintillator and the WLS fiber are
 438 simulated, and the MPPC response is also taken into account. The light yield is smeared
 439 according to statistical fluctuations and electrical noise.

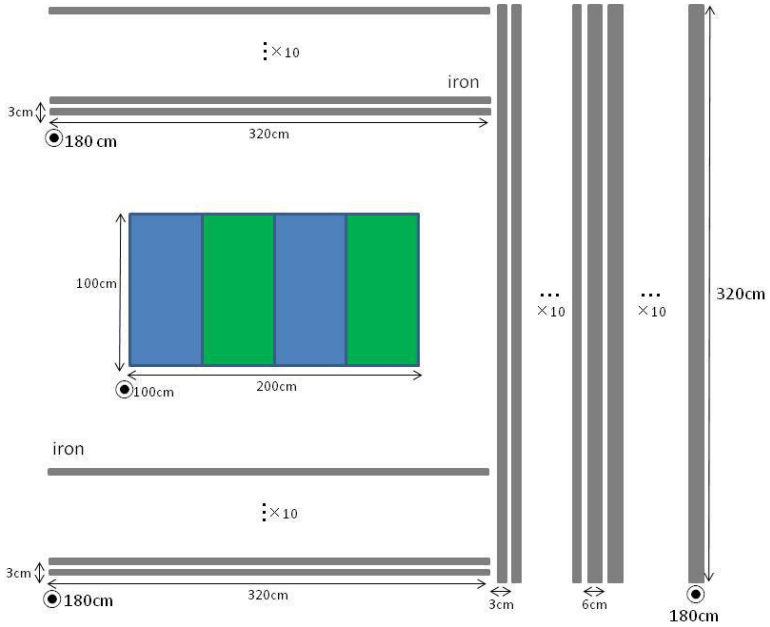


Figure 22: Geometry of the detectors in the Monte Carlo simulation.

440 5.2 Track reconstruction

441 To select neutrino interaction from the hit patterns, a track reconstruction algorithm is
 442 developed. The flow of the track reconstruction is as follows.

- 443 1. Two-dimensional track reconstruction in each sub-detectors
- 444 2. Track matching among the sub-detectors
- 445 3. Three -dimensional track reconstruction

446 Add explanation about two-dim reco, track matching and three-dim reco here.

447 5.3 Event selection

448 First, the events with the track which starts in 5 cm from the wall of the Wagasci module
 449 are rejected to remove the background from the outside.

450 Second, to reject backgrounds from NC and neutral particles, the longest tracks are
 451 required to penetrate more than one (five) iron plates in Side-MRD modules (Baby-MIND).

452 Then, in order to measure muon momentum, the longest tracks are required to stop in
 453 MRDs (Side-MRD modules and Baby-MIND) or penetrate all iron plates.

454 Table 1 and 2 show numbers of the selected events in one water-in Wagasci module
 455 after each event selection in neutrino-mode and antineutrino-mode respectively. As for
 456 the neutrino-mode, 8478 CC events are expected with 1×10^{21} POT, and the purity is
 457 78.0 %. The main background for the neutrino-mode is the neutrino interactions in the
 458 scintillators inside the Wagasci detector. As for the antineutrino-mode, 3331 CC events
 459 are expected with 1×10^{21} POT, and the purity is 59.5 %. The main background for the
 460 antineutrino-mode is the wrong sign contamination from ν_μ events and the antineutrino
 461 interactions in the scintillators inside the Wagasci detector.

Table 1: Expected number of the neutrino-candidate events in one water-in Wagasci module with 1×10^{21} POT in neutrino-mode.

Cut	CC	NC	Scinti Bkg.	Total
Reconstructed	18093.2	699.7	4698.3	23491.2
FV	15150.8	588.4	3934.8	19673.9
Pene. iron	11264.3	237.3	2875.4	14377.0
Stop/Penetrate MRDs	8478.2	214.0	2173.1	10865.2
after all cuts	78.0 %	2.0 %	20.0 %	100 %

Table 2: Expected number of the antineutrino-candidate events in one water-in Wagasci module with 1×10^{21} POT in antineutrino-mode.

Cut	CC	NC	Scinti Bkg.	Wrong sign bkg	Total
Reconstructed	6499.7	107.3	2234.4	2330.8	11172.1
FV	5457.9	89.3	1873.5	1946.6	9367.1
Pene. iron	4172.3	30.8	1440.9	1560.6	7204.6
Stop/Penetrate MRDs	3331.5	28.5	1120.3	1121.2	5601.5
after all cuts	59.5 %	0.5 %	20.0 %	20.0 %	100 %

462 Table 3 and 4 show numbers of the charged-current events in the water-in Wagasci
 463 module after all event selection with a classification based on interactions at a vertex with
 464 1×10^{21} POT in neutrino-mode and antineutrino-mode respectively.

465 Table 5 and 6 show numbers of the charged-current events in one water-in Wagasci
 466 module after all event selection with a classification based on particles after final state
 467 interactions with 1×10^{21} POT in neutrino-mode and antineutrino-mode respectively.

468 Figure 23 and 24 show the reconstructed angles of the longest tracks in the selected
 469 events in the neutrino-mode and the anti-neutrino mode respectively. Figure 25, 26 27

Table 3: Expected number of the charged-current events in the water-in Wagasci module after the event selections with 1×10^{21} POT in neutrino-mode with a classification based on interactions at a vertex.

CCQE	MEC	CCRes	CCDIS	Total
3716.3	747.0	2081.3	1132.3	7676.9
48.4 %	9.7 %	27.1 %	14.7 %	100 %

Table 4: Expected number of the charged-current events in the water-in Wagasci module after the event selections with 1×10^{21} POT in antineutrino-mode with a classification based on interactions at a vertex.

CCQE	MEC	CCRes	CCDIS	Total
2522.0	362.8	765.8	765.8	4416.4
hline 57.1 %	8.2 %	17.3 %	17.3 %	100 %

and 28 show the iron plane numbers in Side-MRD and Baby-MIND corresponding to the end points of the longest tracks in the selected events in the neutrino-mode and the anti-neutrino mode.

5.4 Cross section measurements on water

In the water target events, the background from interaction with scintillators has to be subtracted by using the measurement of the hydrocarbon target.

Table 5: Expected number of the charged-current events in one water-in Wagasci module after the event selections with 1×10^{21} POT in neutrino-mode with a classification based on particles after final state interactions.

CC0 π	CC1 π	CC2 π	CCn π	Total
5423.1	1684.3	242.9	701.1	8051.4
67.4 %	20.9 %	3.0 %	8.7 %	100 %

Table 6: Expected number of the charged-current events in one water-in Wagasci module after the event selections with 1×10^{21} POT in antineutrino-mode with a classification based on particles after final state interactions.

CC0 π	CC1 π	CC2 π	CCn π	Total
2529.3	520.0	37.9	96.0	3183.2
79.5 %	16.3 %	1.2 %	3.0 %	100 %

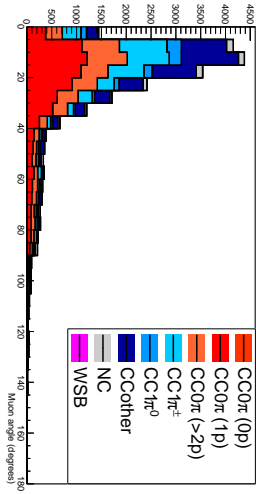


Figure 23: The reconstructed angles of the longest tracks in the selected events in the neutrino-mode.

476 **5.4.1 Charged current cross section measurement**

477 **6 Standalone WAGASCI-module performances**

478 In the previous sections, the WAGASCI detector was studied using the Muon Range Detectors. In this section, the standalone abilities of WAGASCI module are presented. Using
 479 the WAGASCI configuration presented in Section 5, we have evaluated that only 7% of
 480 the muons will be stopped in one of the WAGASCI modules. THowever, this proportion
 481 increases to 53% for pions and 73% for protons produced by neutrino interactions at 1.5°
 482 off-axis. Figure 29 shows the momentum distribution of these daughter particles as well as
 483 for the sub-sample stopped in one of the WAGASCI modules. Therefore, the study of the
 484

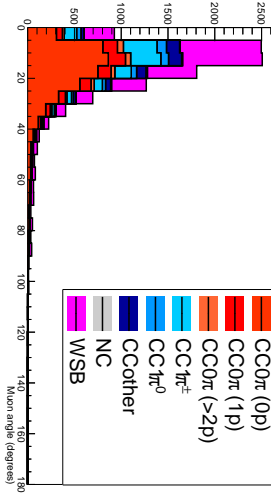


Figure 24: The reconstructed angles of the longest tracks in the selected events in the antineutrino-mode.

485 standalone abilities of the WAGASCI module in this section are dominantly motivated by:

- 486 • the accurate measurement of the neutrino interaction final states. Though most of the
487 muons will be reconstructed and identified in the MRDs, the hadronic particles will
488 predominantly stop in one WAGASCI module. One has therefore to rely exclusively
489 on the WAGASCI module information alone to reconstruct, identify and measure the
490 momentum of pions or protons.
- 491 • the coverage of the MRDs is not 4π . Using the WAGASCI module information can
492 therefore help to constraint the particles that exits the WAGASCI module but do
493 not geometrically enters any MRD.
- 494 • the particle identification of low momenta muons $p_\mu < 300 \text{ MeV}/c$ that will leave only
495 few hits in the MRD. Using the WAGASCI module information will clearly enhance
496 the particle identification.

497 This study is based on an original study done for the ND280 upgrade target, with some
498 modifications. Though the cell size is similar to the WAGASCI configuration presented
499 in Section 5, the external dimensions are different ($186.4 \times 60 \times 130 \text{ cm}^3$). Whenever the
500 results are presented with this external size and this parameter is likely to impact the
501 result, it will be mentioned.

502 Note that in this section, a simplified reconstruction algorithm presented in Section 6.1 is

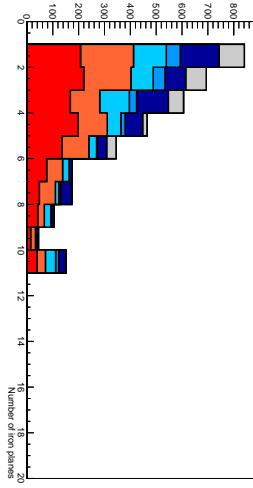


Figure 25: Iron plane numbers in Side-MRD corresponding to the end points of the longest tracks in the selected events in the neutrino-mode.

used. The fiducial volume is chosen accordingly as the inner cube of the module which surfaces are distant of $4 \times$ scintillator space = 10 cm from the module external surfaces. The neutrino interactions are simulated using NEUT v5.3.2. The NEUT input neutrino flux is estimated using JnuBeam v13a and assuming the detector to be located at 1.5° off-axis, as in Section 5. Note that the event reconstruction efficiency as a function of true neutrino energy might be changed at 1.5° , due for example to different Q^2 distributions. For this reason, one has to note that the reconstruction results might slightly be changed from 2.5° and 1.5° . To avoid a similar change on the particle-only reconstruction efficiencies, they will be presented as a function of variables that completely characterize the particle kinematic state, *i.e.* its momentum and angle. Figure 30 shows the vertices distributions of the daughter particles of neutrinos interacting one standard WAGASCI water-module. In this section, we will show the detector reconstruction and particle identification in this phase space, both for leptonic and hadronic particles. We will finally show an empty WAGASCI module can highly enhance the ability to constrain the neutrino interaction final state which is critical to reduce the corresponding uncertainties.

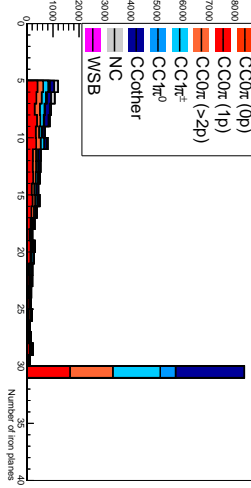


Figure 26: Iron plane numbers in Baby-MIND corresponding to the end points of the longest tracks in the selected events in the neutrino-mode.

518 **6.1 Reconstruction algorithm**

519 **6.1.1 Description**

520 For this section, an ideal “simulated” reconstruction is developed. A particle is recon-
521 structed if:

- 522 1. The particle is charged.
523 2. Lets at least one hit (energy deposit > 2.5 photo-electron) in a scintillator.
524
525 3. The particle enters one TPC and let one hit in the tracker.
526 Or
527

- 528 • The particle should be long enough to be reconstructed by the detector in at
529 least 2 out of 3 views (XZ, YZ, XY). The length criterion requires the particle
530 to let at least 4 hits in the detector. In the “less favourable case” of pure
531 longitudinal or transverse going tracks, it represents a the track length of $L_{track} \geq$
532 $4 \times$ scintillator space = 10.0 cm.
533 • In the views where particles pass the length criterion, the particle shall not
534 be superimposed with longer tracks in at least two views. The superposition

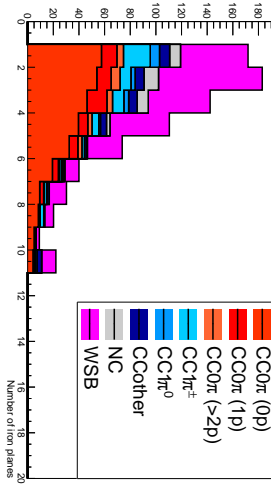


Figure 27: Iron plane numbers in Side-MRD corresponding to the end points of the longest tracks in the selected events in the antineutrino-mode.

535 criterion is estimated with the distance inter-tracks (DIT) which corresponds to
 536 the orthogonal distance between two tracks at the ending point of the shortest
 537 one (see Figure 31). For a track 1, the superposition criterion is tested with
 538 every longer tracks that starts at the same vertex. Let \vec{p}_1 the vector of track
 539 1, and p_1^a its projections in the XZ, YZ and XY planes respectively for $i=1,2,3$.
 540 Note that these are projections in a 2D planes and not on a direction vector. In
 541 this case, the relative angle between the track 1 and a longer track 2 (of vector
 542 \vec{p}_2) in a view a is given by:
 543

$$\cos \theta = \frac{\vec{p}_1^a \cdot \vec{p}_2^a}{\|\vec{p}_1^a\| \|\vec{p}_2^a\|} \quad (1)$$

and the distance inter track is given by:

$$DIT = \|\vec{p}_1^a\| \sin \theta \quad (2)$$

544 The DIT should be higher than $4 \times$ scintillator width for the track 1 to be not
 545 superimposed with the track 2 in the view a, which also corresponds to 10.0 cm
 546 in the nominal configuration.
 547

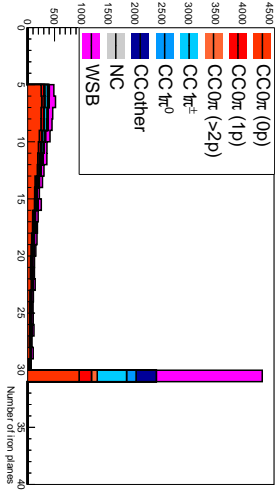


Figure 28: Iron plane numbers in Baby-MIND corresponding to the end points of the longest tracks in the selected events in the antineutrino-mode.

547 6.1.2 Performances

548 The particle-only reconstruction efficiencies and the reconstruction threshold in momenta
 549 are shown in Table 7. This threshold is defined as the maximal momentum for which the
 550 reconstruction efficiency is smaller than 30%. The thresholds in muon and pion momenta
 551 are 150 MeV/c. Most of the muons are above this threshold (see Figure 30) which leads
 552 to a 79% reconstruction efficiency.

	μ	π	p
Reconstruction Efficiency	79%	52%	26%
Momentum threshold	150 MeV/c	150 MeV/c	550 MeV/c

Table 7: Reconstruction efficiency and momentum threshold for muons, pions and protons. The threshold is defined as the maximal momentum for which particles have a reconstruction efficiency smaller than 30%.

553 The lower pion and proton efficiencies (respectively 52% and 26%) are due to lower
 554 efficiencies for similar momenta than muons, coming from strong interactions as shown
 555 on Figures 32. Efficiencies of each particle type tend to decrease in the backward region
 556 due to particle lower momenta. However, for a fixed momentum value, the reconstruc-

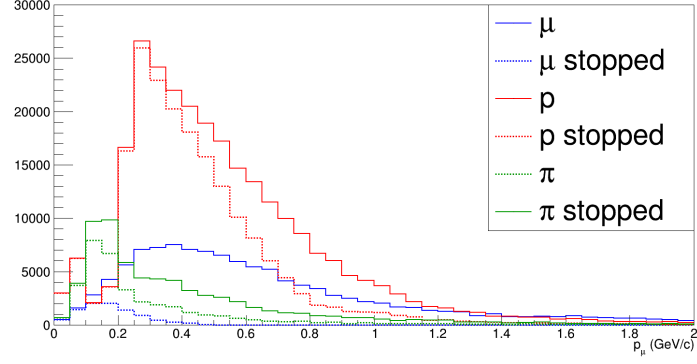


Figure 29: Momentum distribution of true particles in WAGASCI (plain) and corresponding distributions only for particles stopping into the WAGASCI module (dashed).

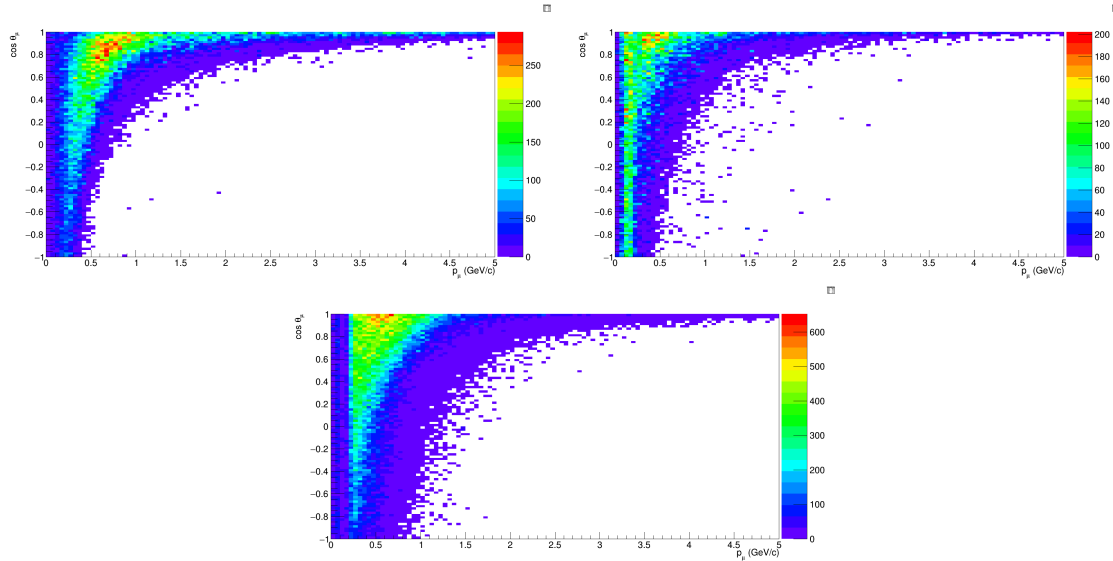


Figure 30: True number of muons (left), charged pions (right) and protons (bottom) in the two WAGASCI water-module as a function of the particles momenta and angles at 1.5° .

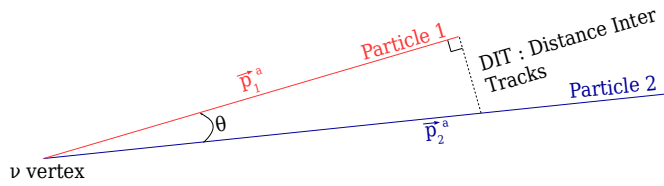


Figure 31: Definition of the distance inter tracks.

tion efficiency is almost uniform which confirms the ability of the WAGASCI detector to reconstruct high angle tracks.

The reconstruction is thereafter tested on neutrino events. Table 8 summarizes the number of reconstructed events and efficiencies for each interaction type. As expected from the high muon reconstruction efficiency, the charged current interactions have reconstruction efficiencies $\geq 85\%$.

	CC0 π	CC1 π	CCOthers	NC	All
Reconstruction efficiency	85%	87%	91%	22%	68%

Table 8: Number of true interactions reconstructed. The purity and reconstruction efficiency of each true interaction is also shown.

The reconstruction efficiencies as a function of the neutrino energy and muon kinematics are respectively shown on Figure 33 and 34.

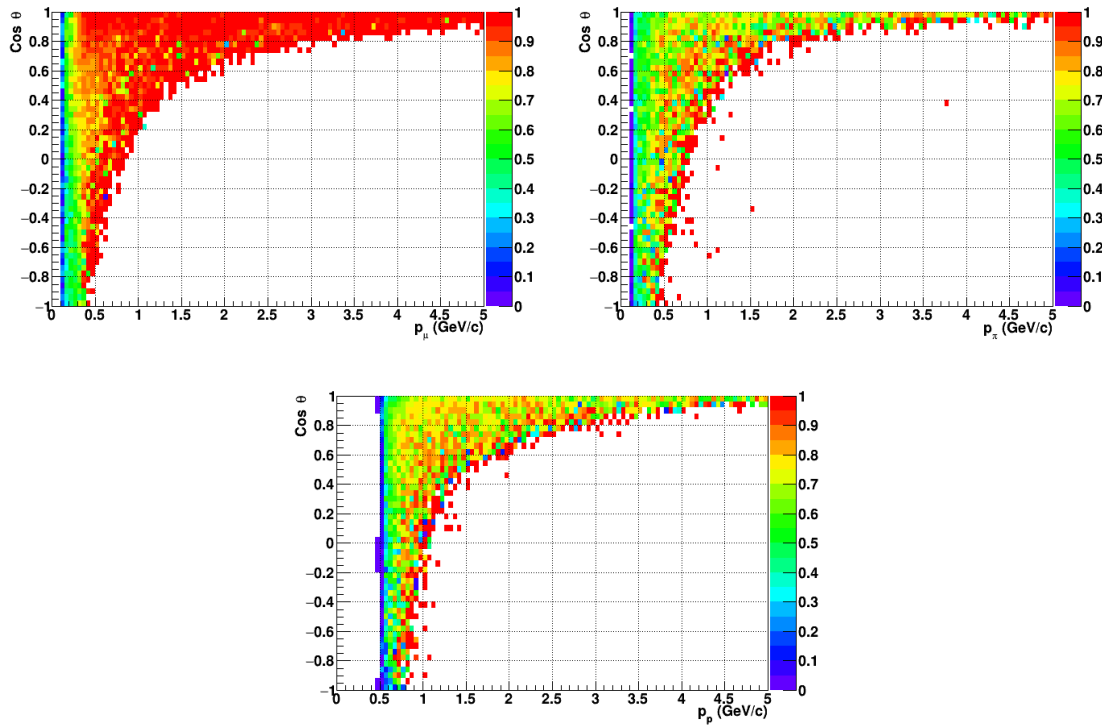


Figure 32: Reconstruction efficiency of muons (left), charged pions (right) and protons (bottom) in the WAGASCI water-module as a function of the particles momenta and angles.

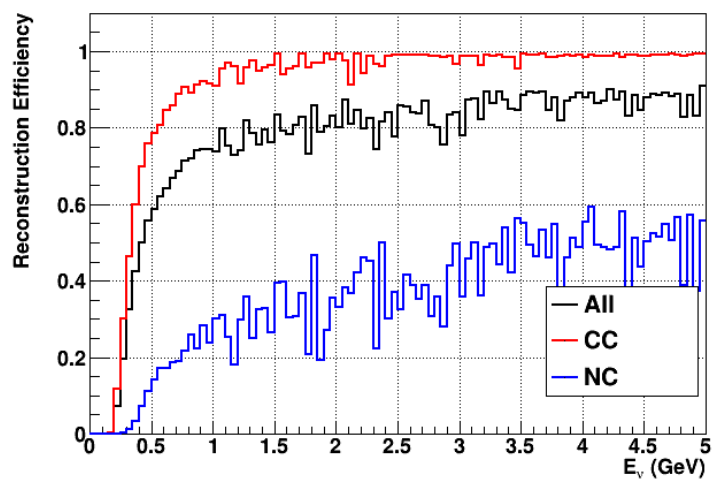


Figure 33: Reconstruction efficiency of all neutrino (black), CC (red) and NC (blue) interactions in the WAGASCI water-module as a function of the neutrino energy.

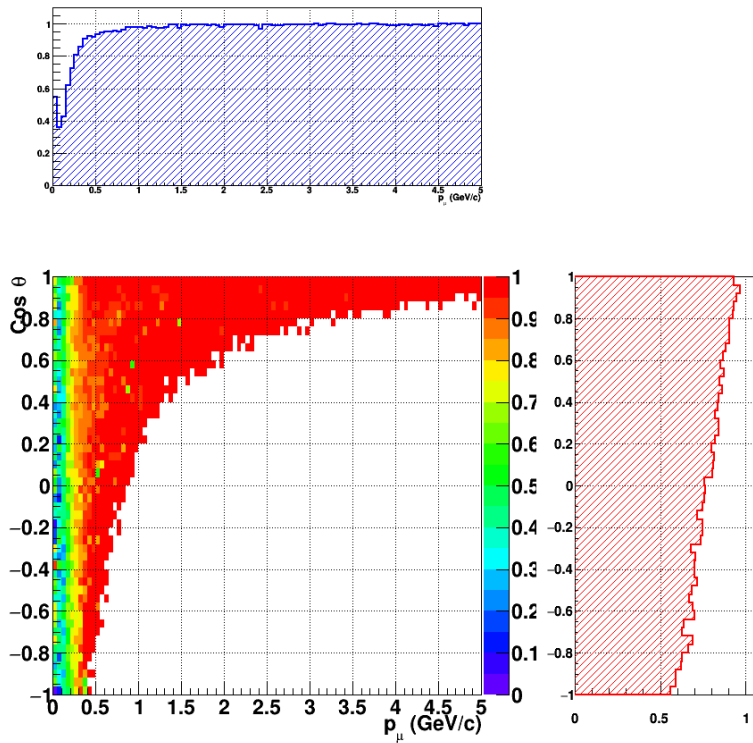


Figure 34: Reconstruction efficiency of CC interactions in the WAGASCI water-module as a function of the muon kinematic variables (momentum and angle).

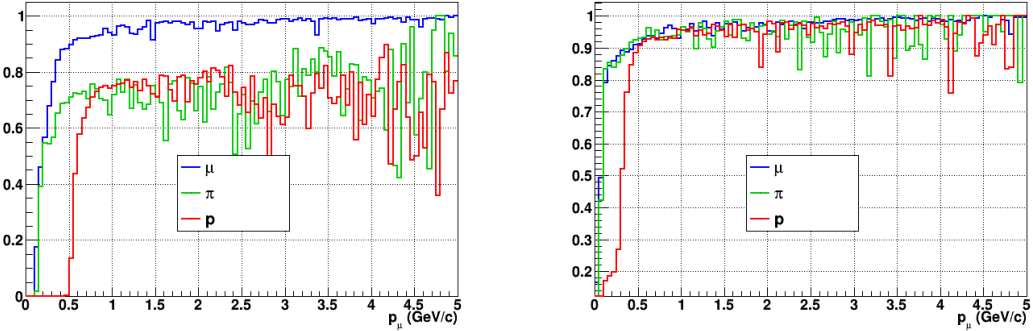


Figure 35: Reconstruction efficiency for muons, pions and protons in the water-in (left) and water-out (right) modules.

Note that a Particle Identification Algorithm has been also developed. It is based on the charge deposition of the particles in the scintillator, of the detection of a decay-electron. However, this information highly depends on the number of scintillator hit by a particle, which creates an important difference between a real WAGASCI module and the one used for the ND280-upgrade simulation. For this reason, the corresponding results will not be detailed here, but can be found in [?].

6.2 Background subtraction: the water-out module

In the nominal configuration, 20% of the neutrino interactions occurs on scintillators (C_8H_8). This background should be removed in order to measure the neutrino interaction on the same target as Super-K, which suppress the differences in cross-section models. For this purpose, we propose to use a water-out module, where the water is replaced by air. The detector is therefore fully active and has a 3 mm spatial resolution (scintillator thickness) which create an ideal detector to reconstruct and identify hadrons, and study np-nh interactions. The counter-part is the difference in particle energy deposition between the water and this water-out module that will need to be corrected for. In this section, we present the capabilities of such a module, and the impact it can have on cross-section measurements for the neutrino community in general and T2K in particular. The same reconstruction and selection as the water-in module is applied. Figure 35 shows the comparison between the water-in and the water-out reconstruction efficiencies for muon, pions and protons. 90% of the muons and 87% of the pions are reconstructed, while 70% of the protons are even reconstructed. It allows to lower down the proton threshold to 250 MeV/c (see Table 9).

As a consequence of tracking even low momenta particle, the reconstruction efficiency is uniform and almost maximal on the entire $\cos \theta_\mu$ phase space, as shown on Figure 36.

	μ	π	p
Reconstruction Efficiency Momentum threshold	90% 50 MeV/c	87% 50 MeV/c	70% 250 MeV/c

Table 9: Reconstruction efficiency, proportions of μ -like and non μ -like and momentum threshold for muons, pions and protons in the empty module. The threshold is defined as the maximal momentum for which particles have a reconstruction efficiency smaller than 20%.

589 Since the fiducial mass represents 0.25 tons, the total number of events is divided by a
 590 factor of 3 compared to the water-in module. The water-out module offers interesting
 591 possibilities to study np-nh interaction since 70% of the protons are reconstructed. In the
 592 future, a possible separation as a function of the number of proton track will be studied.
 593 Moreover, we are currently pursuing the use of single and double transverse variables (cite
 594 Xianguo) to open new possibilities for separating np-nh from Final State Interactions, or
 595 for isolating the interactions on hydrogen from interactions on carbon in this module.

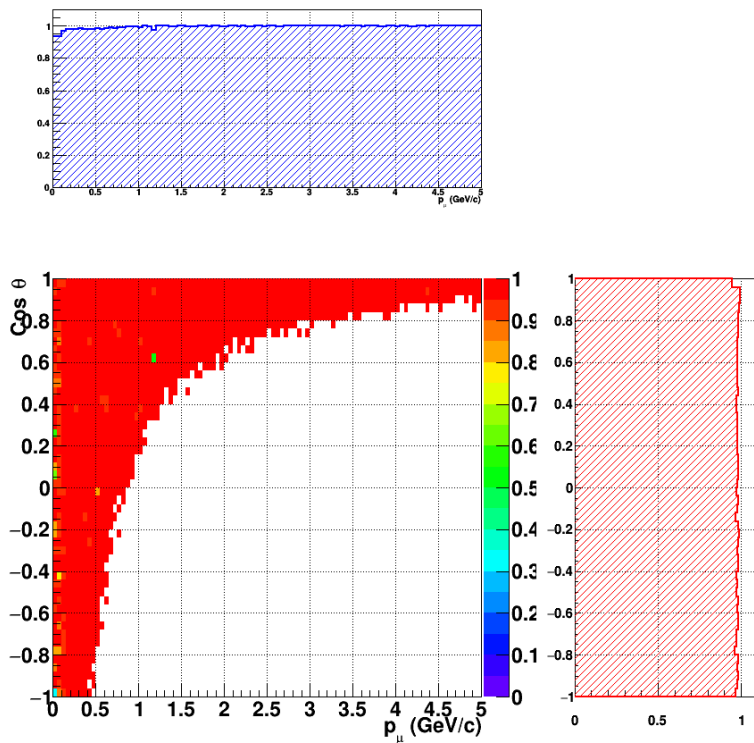


Figure 36: Reconstruction efficiency of CC interactions in the WAGASCI empty module as a function of the muon kinematic variables (momentum and angle).

596 **7 Schedule**

597 We would like to start a physics data taking from T2K beam time after the summer
598 shutdown in 2018. By then, commissioning and tests of the detectors will be completed
599 in J-PARC T59. The experiment can run parasitically with T2K, therefore we request no
600 dedicated beam time nor beam condition as discussed in the following section.

601 Once the approved POT is accumulated, the WAGASCI modules will be removed
602 from the experimental site, but we would like to keep the Baby-MIND and the Side-MRD
603 modules on the B2 floor of the NM pit as common platforms of future neutrino experiments
604 using the T2K neutrino beam.

605 **8 Requests**

606 **8.1 Neutrino beam**

607 The experiment can run parasitically with T2K, therefore we request no dedicated beam
608 time nor beam condition. As data taking periods, we request the ‘nominal’ T2K one-year
609 operation both for the neutrino beam and the antineutrino beam. The T2K has been
610 requesting 0.9×10^{21} POT/year and actually accumulating about 0.7×10^{21} POT/year in
611 recent years. For each year, starting from the Autumn, T2K is running predominantly in
612 the neutrino mode or in the antineutrino mode. Our request is to have one-year neutrino-
613 mode data and another one-year antineutrino mode data assuming that the POT for the
614 fast extraction in each year is more than 0.5×10^{21} POT.

615 **8.2 Equipment request including power line**

616 We request the followings in terms of equipment on the B2 floor:

- 617 • Site for the WAGASCI modules, Side-MRD modules and BabyMIND and their elec-
618 tronics system on the B2 floor of the near detector hall (Fig. 3).
- 619 • Anchor points (holes) on the B2 floor to secure the WAGASCI modules, Side-MRD
620 module and Baby-MIND (Fig. ??)
- 621 • Power line for the magnets in Baby-MIND: 400 V tri-phase 48-to-62 Hz, capable of
622 delivering 12 kW.
- 623 • Electricity for electronics and water circulation system, 3 kW, standard Japanese
624 electrical sockets.
 - 625 1. Online PCs: 2.1 kW
 - 626 2. Electronics: 0.7 kW
 - 627 3. Water sensors: ?

- 628 • Air conditioner for cooling heat generation at Baby-MIND magnets, online PCs and
629 electronics
- 630 • Beam timing signal and spill information
- 631 • Network connection

632 **8.2.1 Baby MIND Equipment request including power line**

633 We request the following in terms of equipment on the B2 floor:

- 634 • Site for the Baby MIND detector and its electronics systems on the B2 floor of the
635 near detector hall.
- 636 • Anchor points (holes) on the B2 floor to secure the 9 support frames, of order 4 holes
637 per frame, detailed floor plans to be communicated in a separate document.
- 638 • Power line for the magnet: 400 V tri-phase 48-to-62 Hz, capable of delivering 12
639 kW. We have a wish for the magnet power line to be installed and available to us by
640 beginning of March 2018.
- 641 • Electricity for electronics, 1 kW, standard Japanese electrical sockets.
- 642 • Beam timing signal and spill information
- 643 • Network connection

644 The infrastructure for much of the above exists already, and will be shared in part with
645 the WAGASCI experiment. Exceptions are the power line for the magnet and holes in the
646 B2 floor to anchor the detector support structures.

647 **9 Conclusion**

648 **References**

- 649 [1] K. Abe et al. Measurement of the muon neutrino inclusive charged-current cross sec-
650 tion in the energy range of 13 GeV with the T2K INGRID detector. *Phys. Rev.*,
651 D93(7):072002, 2016.
- 652 [2] M. Antonova et al. Baby MIND Experiment Construction Status. In *Prospects in*
653 *Neutrino Physics (NuPhys2016) London, London, United Kingdom, December 12-14,*
654 2016, 2017.

- 655 [3] J. Fleury, S. Callier, C. de La Taille, N. Seguin, D. Thienpont, F. Dulucq, S. Ahmad,
656 and G. Martin. Petiroc and Citiroc: front-end ASICs for SiPM read-out and ToF
657 applications. *JINST*, 9:C01049, 2014.
- 658 [4] Yu. G. Kudenko, L. S. Littenberg, V. A. Mayatsky, O. V. Mineev, and N. V. Ershov.
659 Extruded plastic counters with WLS fiber readout. *Nucl. Instrum. Meth.*, A469:340–
660 346, 2001.
- 661 [5] O. Mineev, Yu. Kudenko, Yu. Musienko, I. Polyansky, and N. Yershov. Scintillator
662 detectors with long WLS fibers and multi-pixel photodiodes. *JINST*, 6:P12004, 2011.
- 663 [6] Etam Noah et al. Readout scheme for the Baby-MIND detector. *PoS*, Photo-
664 toDet2015:031, 2016.